In Vivo Three-Dimensional Lamina Cribrosa Strains in Healthy, Ocular Hypertensive, and Glaucoma Eyes Following Acute Intraocular Pressure Elevation

Meghna R. Beotra,[1] Xiaofei Wang,[1] Tin A. Tun,[1,2] Liang Zhang,[1] Mani Baskaran,[2,3] Tin Aung,[2–4] Nicholas G. Strouthidis,[2,5,6] and Michaël J. A. Girard[1,2]

[1]Ophthalmic Engineering & Innovation Laboratory, Department of Biomedical Engineering, Faculty of Engineering, National University of Singapore, Singapore
[2]Singapore Eye Research Institute, Singapore National Eye Centre, Singapore
[3]Duke-NUS Medical School, Singapore
[4]Department of Ophthalmology, Yong Loo Lin School of Medicine, National University of Singapore, Singapore
[5]NIHR Biomedical Research Centre, Moorfields Eye Hospital NHS Foundation Trust and UCL Institute of Ophthalmology, London, United Kingdom
[6]Discipline of Clinical Ophthalmology and Eye Health, University of Sydney, Sydney, New South Wales, Australia

Correspondence: Michaël J.A. Girard, Ophthalmic Engineering & Innovation Laboratory, Department of Biomedical Engineering, National University of Singapore, Engineering Block 4, #04-8, 4 Engineering Drive 3, Singapore 117583; mgirard@nus.edu.sg.

Submitted: April 2, 2017
Accepted: November 14, 2017

Citation: Beotra MR, Wang X, Tun TA, et al. In vivo three-dimensional lamina cribrosa strains in healthy, ocular hypertensive, and glaucoma eyes following acute intraocular pressure elevation. *Invest Ophthalmol Vis Sci*. 2018;59:260–272. https://doi.org/10.1167/iovs.17-21982

Purpose. To compare in vivo lamina cribrosa (LC) strains (deformations) following acute IOP elevation in healthy, glaucoma, and ocular hypertensive subjects.

Methods. There were 20 healthy, 20 high-tension primary open-angle glaucoma (POAG), 16 primary angle-closure glaucoma (PACG), and 20 ocular hypertensive (OHT; with normal visual fields) eyes studied. For each test eye, the optic nerve head was imaged three times (at baseline IOP, following an acute elevation of IOP to approximately 35 then 45 mm Hg using an ophthalmodynamomter) using optical coherence tomography (OCT). A three-dimensional (3D) strain-mapping algorithm was applied to both sets of baseline and IOP-elevated OCT volumes to extract IOP-induced 3D strains. Octant-wise LC strains were also extracted to study the pattern of local deformation.

Results. The average LC strain in OHT subjects (3.96%) was significantly lower than that measured in healthy subjects (6.81%; $P < 0.05$). On average, POAG subjects experienced higher strain than the PACG subjects (4.05%), healthy subjects experienced higher strains than the POAG and PACG subjects, but these difference were not statistically significant. Local LC deformations showed lowest strain in the infero-temporal and temporal octant in the POAG and OHT subjects.

Conclusions. We demonstrate measurable LC strains in vivo in humans as a response to acute IOP elevation. In this population, our data suggest that OHT LCs experience lower IOP-induced strains than healthy LCs.

Keywords: strain mapping, lamina cribrosa, glaucoma, ocular hypertension, intraocular pressure

Glaucoma is a heterogeneous optic neuropathy, characterized by retinal ganglion cell (RGC) axon damage in the lamina cribrosa (LC).[1,2] The event of RGC axon damage may be explained by the interaction of IOP and cerebrospinal fluid pressure (CSFP).[3] Elevated IOP could damage the RGC axons (either directly or indirectly) and alter LC microcapillary blood flow in the optic nerve head (ONH). However, not all patients with high IOP (ocular hypertension [OHT]) develop glaucomatous optic neuropathy[4,5]—the etiology of which remains unknown. In brief, our current understanding of glaucoma is insufficient: we know that IOP is important, but it is clearly not the only risk factor in the development and progression of this disease. Recently, the role of tissue biomechanics has been identified[6–8] and it was hypothesized that IOP (or other loads such as cerebro-spinal fluid pressure [CSFP][9] and optic nerve traction[10–12]) deforms the ONH, particularly the LC. These deformations may directly alter the hemodynamics within the ONH, and drive RGC axon damage and death.[6] Thus, the central idea of the biomechanical theory is that strains (i.e., deformations) of the ONH tissues (particularly the LC) might indicate the IOP level it can sustain and therefore play an important role in early diagnosis and better clinical management of glaucomatous changes. For instance, ONH biomechanics could become a strong diagnostic marker to predict those at higher risks of developing glaucoma. This would be especially useful for OHT subjects. Biomechanics may also yield explanations for why normal tension glaucoma subjects develop glaucoma at normal levels of IOP, and may even lead the way to new therapeutic approaches to alter ONH biomechanics in vivo.[13]

However, current techniques to measure LC deformations clinically are limited. Some in vivo studies[14–16] have reported changes in LC depth as a surrogate for LC deformations. LC depth is typically measured with optical coherence tomogra-

phy (OCT) as the average or maximum distance between the plane of Bruch's membrane opening (BMO) and the anterior LC surface.[15] However, LC depth (or its change with IOP) is a poor surrogate for LC deformations as the peripapillary tissues ineluctably influence it. For instance, following an acute elevation of IOP, an eye exhibiting a decrease in choroidal thickness (but no LC deformations) would also exhibit a decrease in LC depth. In addition, the LC could exhibit significant deformations (high compressive strain, or stretch along a direction parallel to the plane of BMO) that would yield no changes in LC depth. Other OCT-derived parameters such as the curvature and the global shape index of the LC (and their changes with IOP) have also been proposed.[17,18] While such parameters may be of clinical interest to classify glaucoma severity, they are not representative of strain (the engineering definition of deformation) that could indicate local compression, shear, or stretch of the axons passing through the LC.

Recently, we have developed an OCT-based three-dimensional (3D) strain mapping technology to characterize ONH deformations.[19,20] Using this technology, we have demonstrated that local ONH displacements and strains could be measured in vivo and that trabeculectomy significantly relieved strain levels in the LC.[20] We also found that the eyes exhibiting the most severe visual field loss were the ones exhibiting the highest LC strain relief following trabeculectomy. This suggests a potential role for LC strain in the development and progression of glaucoma.

The aim of this study was to further characterize the in vivo biomechanical response of the LC, but this time after acute IOP loading (induced via ophthalmodynamometry). Our goal was to understand whether there exist variations in IOP-induced LC strains between healthy, ocular hypertensive, and glaucoma eyes.

Methods

Subject Recruitment

There were 76 Chinese subjects recruited for a 2-year longitudinal study at the Singapore National Eye Center, Singapore. Among the recruited subjects, 20 had high-tension primary open-angle glaucoma (POAG), 16 had primary angle-closure glaucoma (PACG), 20 had ocular hypertension (OHT), and 20 were healthy controls. In this study, subject data from the first visit (baseline visit) of all the subjects were used.

Glaucoma was defined by the presence of glaucomatous optic neuropathy (GON), which is associated with a vertical cup-disc ratio >0.7 and/or narrowing of the neuroretinal rim along with presence of visual field defects in standard automated perimetry (SAP). Visual field defects are found in the presence of (1) glaucoma hemifield test outside normal limits, (2) a cluster of ≥ 3, nonedge, contiguous points on the pattern deviation plot, not crossing the horizontal meridian with a probability of $<5\%$ being present in age-matched normals (one of which was $<1\%$), and (3) pattern standard deviation <0.05; these were repeatable on two separate occasions, in association with a closed angle (PACG) or with an open angle (POAG). Reliability criteria for SAP were defined as $<20\%$ fixation losses, $<33\%$ false-negative error, and $<33\%$ false-positive error. All glaucoma subjects had IOP >21 mm Hg at least once after they were clinically diagnosed with GON. OHT was defined by the presence of high IOP (>21 mm Hg), open angles in the absence of GON or visual field loss. All glaucoma subjects were on IOP lowering medications, except for two that were newly diagnosed. This is why glaucoma subjects may exhibit IOPs <21 mm Hg at the time of this study, but all presented elevated IOP before medication. Subjects with ocular hypertension were under observation and not under medication. All PACG eyes had undergone laser peripheral iridotomy prior to recruitment into the study.

Inclusion criteria were subjects aged ≥ 50 years, with no known history of intraocular surgery. Subjects with visual field deficits related to diabetic retinopathy or any other optic neuropathies, advanced glaucoma precluding acute elevation of IOP were excluded. The study was approved by the SingHealth Centralized institutional review board, and adhered to the tenets of the Declaration of Helsinki. Written informed consent was obtained from all subjects.

Clinical Examination of Subjects

All recruited subjects underwent the following examinations in both eyes: (1) measurement of visual acuity, (2) refraction using an autokeratometer (RK-5; Canon, Tokyo, Japan), (3) slit-lamp biomicroscopy (model BQ-900; Haag-Streit, Köniz, Switzerland), (4) Goldmann applanation tonometry (AT900D; Haag-Streit), (5) dark-room four-mirror gonioscopy (Ocular Instruments, Inc., Bellevue, WA, USA), (6) SAP (SITA-Standard 24-2 program, Humphrey Field Analyzer II-750i; Carl Zeiss Meditec, Dublin, CA, USA), and (7), IOP measurements with a Tonopen AVIA applanation tonometer (Reichert, Inc., Depew, NY, USA). The study eye was chosen as the one (1) with unilateral glaucoma, (2) with a higher mean deviation (MD) from SAP in bilateral glaucoma, or (3) at random in healthy subjects and subjects with equal severity of glaucoma in both eyes.

Acute Elevations of Intraocular Pressure and Optical Coherence Tomography Imaging

For the study eye of each subject, the IOP was measured using a Tonopen post pupillary dilation with tropicamide 1% (Alcon, Puurs, Belgium) and an OCT volume of the ONH (Volume 1) was acquired at baseline IOP using spectral-domain OCT (Spectralis; Heidelberg Engineering GmbH, Heidelberg, Germany).[17] The IOP was then raised by gentle indentation of the temporal side of the lower eyelid (perpendicular to the sclera), using an ophthalmodynamometer (spring-load indenter). After this first IOP increment, IOP was held constant and was measured with a Tonopen while the indenter was maintained in place to acquire the second OCT volume (Volume 2). This was repeated with a larger indentation force to establish a higher IOP increment followed by acquiring the third OCT volume (Volume 3). The forces for IOP increase were chosen to correspond to final IOP values of approximately 35 and 45 mm Hg, respectively (based on a preliminary assessment performed on 20 healthy eyes).[17] The applied forces were consistently 0.64 N (82.5 g) and 0.9 N (95 g) as calibrated using a uniaxial tensile tester (Instron-5848; Instron, Inc., Noorwood, MA, USA).

For each test eye, the acquired OCT volumes were grouped into 2 sets (Set 1: Volume 1 at baseline IOP [undeformed] + Volume 2 at first IOP elevation [deformed], Set 2: Volume 1 at baseline IOP [undeformed] + Volume 3 at second IOP elevation [deformed]) in order to extract tissue deformation at both levels of IOP loading. Each OCT volume consisted of 97 serial horizontal B-scans (30-μm distance between B-scans; 384 A-scans per B-scan; ×20 B-scan averaging) that covered a rectangular area of $15° \times 10°$ centered on the ONH. The eye tracking and enhanced-depth imaging modalities of the Spectralis were used during image acquisition.

Investigative Ophthalmology & Visual Science

Improving OCT Image Quality Using Adaptive Compensation

To improve LC visibility, all OCT volumes were processed using adaptive compensation.[19,20] Adaptive compensation is a postprocessing technique used to improve tissue visibility at high depth and below blood vessel shadows,[21,22] and to increase tissue contrast so as to facilitate manual segmentation of ONH tissues.

Digital Reconstruction of the LC

Each compensated baseline (lowest IOP) OCT volume was manually segmented (i.e., delineated) to identify BMO and the LC using Amira (version 5.6; FEI, Hillsboro, OR, USA) through an established protocol.[20] The following was noted: (1) BMO was delineated to construct the BMO plane, with respect to which all axial LC displacements were calculated; and (2) LC segmentations were conducted uniformly up to the depth of 135 μm only when the anterior LC was visible as detected from the OCT signal postprocessed with adaptive compensation. This depth was chosen because the visibility of the LC tissue was consistently good (based on visual assessment) in all scans.

Exclusion Criterion for Subjects With Low Lamina Cribrosa Visibility

In this study, we excluded the OCT volume sets in which at least one OCT volume exhibited low LC visibility (i.e., en face LC visibility <60% of the total BMO area). For instance, if Volume 1 (undeformed) exhibited poor LC visibility, both Set 1 and Set 2 were excluded (since Volume 1 is part of both sets). However, if Volume 3 (deformed) exhibited poor LC visibility, Set 2 was excluded (since Volume 3 is a part of Set 2 only), whereas Set 1 was included.

Rigid Alignment of OCT Volumes to Improve Strain Mapping Efficiency

To enhance the efficiency of 3D strain mapping, each deformed OCT volume (at elevated IOPs) were first oriented to best align with the undeformed OCT volume (at baseline IOP) using the software Amira. This was done to reduce 3D rigid translation/rotation between the two OCT volumes (as could occur due to patient's head/eye movements between scanning sessions), the aligned OCT volumes were then processed (as described below) to extract the 3D deformation (quantified as strain).

Three-Dimensional LC Displacement and Strain Mapping

We applied our 3D tracking algorithm[19,20] to each set of OCT volumes (from the undeformed volume to the deformed volume in Set 1 and Set 2) in order to extract IOP-induced (1) axial LC displacements, and (2) LC strains. For each set of two OCT volumes (undeformed and deformed), the BMO planes of both volumes were matched to remove any leftover rigid body motion; we then calculated the axial displacement for each LC point as the component of the 3D LC displacement vector that was perpendicular to the BMO planes (convention: negative values indicate posterior axial LC displacements and positive values indicate anterior axial LC displacements). In this study, effective strain is reported as the state of deformation of the laminar tissues as a result of IOP loading.

Note that the effective strain is a single index that conveniently summarizes the 3D state of strain at a local tissue point, and that takes into account both compressive and tensile effects. In other words, the higher the compressive or tensile strain, the higher the effective strain. The effective strain E_{Eff} can be expressed as

$$E_{\text{Eff}} = \sqrt{\frac{(E_1 - E_2)^2 + (E_1 - E_3)^2 + (E_2 - E_3)^2}{2}}, \qquad (1)$$

where, E_1, E_2, and E_3 are the principal components of the Green–Lagrange strain tensor. The details of the 3D strain mapping principle and the parameters used in this algorithm to increase accuracy and efficiency can be referred to from Girard et al.[19,20] Note that the values reported for effective strain and axial displacement at both the first and the second IOP elevation are calculated with respect to the baseline IOP (undeformed) OCT volume.

Retinal Nerve Fiber Layer Thickness

We also measured retinal nerve fiber layer (RNFL) thickness (nasally and temporally) 2 mm away from the BMO center in the central horizontal B-Scan. We reported the average RNFL thickness for each eye at baseline. Note that we could not measure RNFL thickness consistently in the inferior and superior regions because our scans were shorter along the superior-inferior direction.

Statistical Analysis

To study the effect of acute IOP elevations on LC deformations, statistical analysis was performed using R (version 3.0.2; R Foundation, Vienna, Austria). Strain and displacement were defined as continuous variables, whereas diagnosis was defined as a categoric variable with four levels (healthy, POAG, PACG, OHT). We used the analysis of covariance (ANCOVA) with post hoc Tukey test to compare the median values of LC strain and displacements between different diagnostic groups after adjusting for age, sex, and baseline IOP. We used Wilcoxon Signed Ranks test to study the differences in median LC strain and displacement values at different IOP elevations. To study the effect of acute IOP elevations on local LC deformations, the LCs of all the eyes were divided into eight regions of 45° (with respect to the center of the BMO ellipse). Strain was defined as a continuous variable, whereas position of the octant was defined as a categoric variable with eight categories (superior, supero-temporal, temporal, infero-temporal, inferior, infero-nasal, nasal, supero-nasal). The median values of the strains were extracted for each octant of the LC. These strain values were analyzed using generalized estimating equations (GEE), in order to account for intraoctant associations while analyzing differences between different octants of the LCs. Statistical significance level was set at 0.05. To ensure there was no bias from octants with poor LC visibility, we removed octants with <50% LC visibility from our analysis.

Results

Demographics and IOP

A total of 76 Chinese subjects were recruited, of whom seven were excluded because they had low en face LC visibility (<60% of the BMO area). From the remaining 69 subjects, one subject showed low en face LC visibility in the first IOP elevation OCT volume and five subjects showed low en face LC visibility in the second IOP elevation OCT volume. The

sets comprising these volumes were excluded. Therefore, a total of 66 subjects (healthy: 17, POAG: 19, PACG: 15, OHT: 17) were included in the first IOP elevation and 62 subjects (healthy: 13, POAG: 19, PACG: 15, OHT: 17) in the second IOP elevation.

Subjects with PACG were significantly older (68 ± 5) than healthy (58 ± 4; $P < 0.05$) and OHT subjects (59.8 ± 4.91; $P < 0.05$); POAG subjects (64 ± 8; $P < 0.05$) were older than healthy subjects. Baseline IOP was significantly higher in OHT subjects (21 ± 2.68 mm Hg) than in PACG subjects (17 ± 4 mm Hg) or healthy subjects (17 ± 3 mm Hg) (Table 1). The mean IOP of all study subjects at baseline was 18.37 ± 3.58 mm Hg, which increased to 37.84 ± 6.09 (first elevation) and then 46.55 ± 6.32 mm Hg (second elevation), respectively. For each diagnostic group, the IOP was significantly higher at first and second elevation than at baseline (all $P < 0.001$).

IOP-Induced Displacements

In response to the first IOP elevation, the LC displaced posteriorly (on average) in all groups (Table 1). In response to the second IOP elevation, axial LC displacements for POAG eyes (–5.33 ± 6.25 μm; $P = 0.02$) were significantly different from those achieved in response to the first IOP elevation (–2.8 ± 3.59 μm). In response to the second IOP elevation, POAG LCs also exhibited a significantly larger posterior displacement (–5.33 ± 6.25 μm; $P = 0.025$) compared with OHT (–0.66 ± 4.47 μm) LCs.

IOP-Induced Effective Strains

For the first IOP elevation, the OHT subjects exhibited significantly lower median effective strain (3.96% ± 2.81%; Fig. 1) than in healthy subjects (6.81% ± 3.31%; $P = 0.045$). For the second IOP elevation, no differences were found between groups ($P > 0.05$ for all comparisons). While the median LC strains were lower in POAG and PACG subjects than in healthy subjects, we found no statistical significant differences ($P > 0.99$ and $P = 0.071$, respectively). Representative maps of IOP-induced LC strains for each subject group and for the first IOP elevation are shown in Figure 2.

Median LC effective strains induced by first and second IOP elevation are shown as scatterplots in Figure 3 as a function of age, functional loss (MD of visual field), RNFL thickness (average), and IOP. Within each group, the LC strains at the second IOP elevation were not significantly different from those observed at the first IOP elevation suggesting nonlinear strain behavior with IOP ($P > 0.05$ for all groups). For any IOP elevation, we found no associations between strain and age, and between strain and functional loss ($P > 0.05$). For any given group, we found no associations between strain and the magnitude of the first (or second) IOP increase ($P > 0.05$ for all groups). Finally, we found that strain was positively associated with RNFL thickness for the first IOP elevation only ($P < 0.05$).

Regional Variations in LC Effective Strains

Regional variations in LC effective strains (median) for all groups are tabulated in Table 2 and are diagrammatically presented in Figure 4. In healthy subjects, we found no significant differences in effective strain across sectors for both IOP elevations ($P > 0.05$).

For the first IOP elevation in POAG subjects, we observed significantly lower effective strain in the temporal (5.29%), infero-temporal (4.97%), and inferior (5.14%) sectors than in the supero-nasal sector (6.80%; all $P < 0.05$).

Table 1. Demographics and Clinical Characteristics of Included Study Subjects

Characteristic	Mean (SD) or *n* (%)				*P* Value				
	Healthy	POAG	PACG	OHT	Healthy-POAG	Healthy-PACG	Healthy-OHT	PACG-POAG	OHT-POAG	PACG-OHT
Age, y	58 ± 4	64 ± 8	68 ± 5	59.8 ± 4.91	0.004	2.3^{e-05}	1	0.45	0.12	0.001
Sex, female (%)	14 (82)	2 (11)	5 (33.3)	12 (75)	6.4^{e-05}	0.01	1	1	0.001	0.09
Study eye, OD (%)	11 (65)	8 (42)	9 (60)	8 (50)	1	1	1	1	1	1
VCDR	0.39 ± 0.08	0.74 ± 0.12	0.75 ± 0.15	0.5 ± 0.12	6.9^{e-12}	6.8^{e-11}	0.005	1	8.7^{e-06}	1.8^{e-05}
Visual field, MD (dB)	–2.21 ± 2.56	–4.61 ± 4.92	–5.25 ± 3.61	–1.58 ± 2.46	0.63	0.26	1	1	0.13	0.041
Average RNFL thickness (μm)	68.88 ± 9.83	58.25 ± 11.63	60.25 ± 9.16	64.66 ± 10.48	0.019	0.13	1	1	0.41	1
IOP, mm Hg										
Baseline	17 ± 3	18 ± 4	17 ± 4	21 ± 2.68	1	1	0.008	1	0.16	0.015
At elevation 1	38 ± 6	36 ± 5	35 ± 7	42 ± 4.92	1	1	0.17	1	0.06	0.026
At elevation 2	46 ± 8	45 ± 6	46 ± 6	49 ± 4.37	1	1	1	1	1	1
Effective strain (%)										
Baseline – IOP elevation 1	6.81 ± 3.31	6.04 ± 3.31	4.05 ± 2.40	3.96 ± 2.81	0.7	0.11	0.036	0.46	0.43	0.99
Baseline – IOP elevation 2	5.87 ± 3.75	6.33 ± 3.27	4.89 ± 2.95	3.80 ± 2.70	0.99	0.68	0.18	0.71	0.30	0.89
Axial displacement perpendicular to BMO (μm)										
Baseline – IOP elevation 1	–3.55 ± 4.48	–2.80 ± 3.59	–1.25 ± 1.75	–1.14 ± 2.27	0.99	0.36	0.16	0.29	0.25	0.99
Baseline – IOP elevation 2	–3.63 ± 4.08	–5.33 ± 6.25	–1.41 ± 2.67	–0.66 ± 4.47	0.63	0.91	0.56	0.12	0.048	0.95

VCDR, vertical cup to disc ratio.

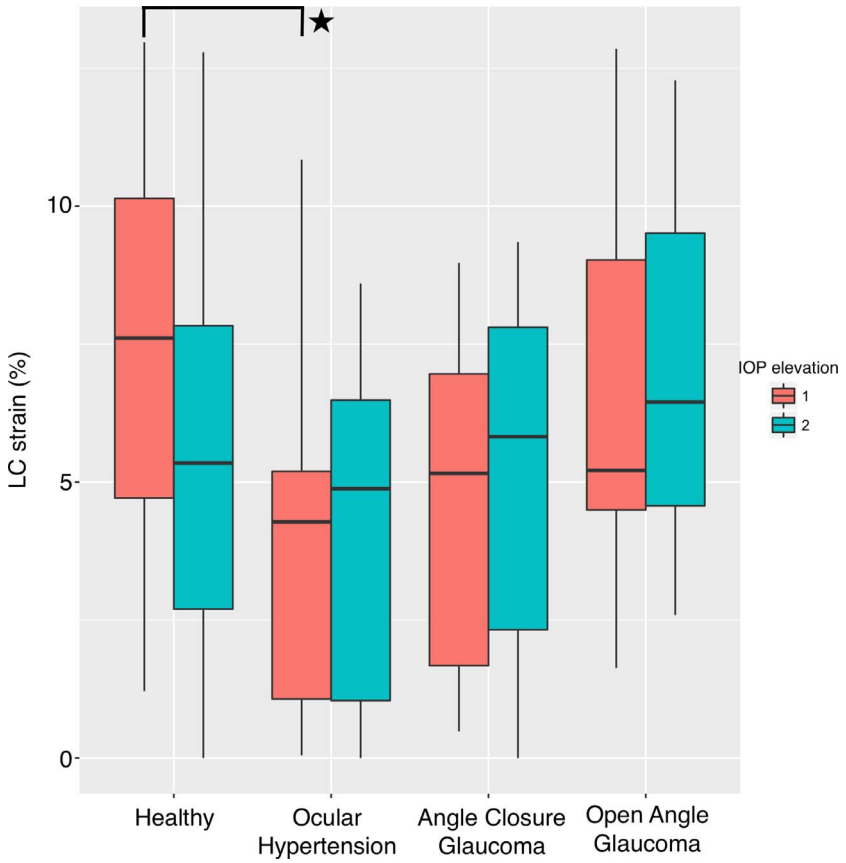

Figure 1. Box plot of median LC effective strains induced by IOP elevations across diagnostic groups (healthy, OHT, PACG, POAG). ★ represents statistically significant difference between LC strains induced by the first IOP elevation in healthy and OHT groups with a P value < 0.05.

For the first IOP elevation in PACG subjects, we observed significantly lower effective strain in the infero-temporal (3.52%) and inferior (3.07%) sectors than in the superior (4.20%) sector ($P < 0.05$). Effective strain in the temporal sector (3.70%) was also significantly lower (all $P < 0.05$) than in the supero-temporal (4.29%) and superior (4.20%) sectors.

For the first IOP elevation in OHT subjects, the supero-temporal region (3.48%; all $P < 0.05$) experienced significantly lower strain than the nasal half of the LC; the nasal region (5.70%; all $P < 0.05$) and infero-nasal region (4.83%; all $P < 0.05$) experienced higher strain than the temporal half of the eye.

No significant differences were found across sectors in POAG, PACG, and OHT subjects for the second IOP elevation (all $P > 0.05$).

Discussion

In this study, we have combined 3D strain mapping technology and in vivo OCT imaging of the ONH to: (1) quantitatively map 3D LC strains in response to acute IOP elevations, (2) compare these LC strains between diagnostic classifications, and (3) assess regional differences in IOP-induced LC strain. We found that OHT subjects exhibited significantly lower LC effective strains than healthy subjects. Regional variations in 3D strain pattern were also found, with infero-temporal and temporal sectors showing the lowest deformation in POAG subjects.

For each diagnostic group, we found that the LC strains at the second IOP elevation were not significantly different from those observed at the first IOP elevation suggesting a possible nonlinear strain behavior with IOP. This could be explained by the nonlinear stress-strain behavior of collagen fibers present in the LC; which has not been extensively studied. This could also be attributed to the surrounding nonlinear sclera. Studies have shown that the sclera, when exposed to acute elevations of IOP, can considerably stiffen when IOP increases beyond 30 mm Hg.[23] It has been suggested that scleral stiffening with IOP might be a protective mechanism that minimizes deformations near the ONH (i.e., in the LC).

In this study, we found that OHT subjects experienced significantly lower LC effective strains than healthy subjects. Our results are consistent with our previous study where we reported negligible IOP-induced LC shape changes in the same set of OHT subjects.[17] How could this be explained? First, it is possible that OHT subjects would have stiffer ONH connective tissues. For instance, stiff scleras and/or stiff LCs should in principle result in smaller IOP-induced LC deformations.[24] Second, OHT subjects may have specific ONH morphologies and/or collagen fiber arrangements that could also limit IOP-induced LC deformations.[25] For instance, if OHT subjects exhibit small collagen crimp for normal/physiological IOP levels, this could considerably reduce their connective tissue deformations for higher IOPs (Sigal I, et al. *IOVS* 2013;54:ARVO E-Abstract 3158). Third, a higher CSFP that opposes the IOP at the level of the LC, could also lead to negligible LC deformations. Interestingly, high CSFP has been estimated in OHT subjects in the Beijing Eye Study.[26] Overall, this resistance to deformation could potentially explain why OHT eyes can withstand elevated IOP levels without developing glaucomatous changes in the ONH.[4,5] Larger cross-sectional and longitudinal studies are however needed

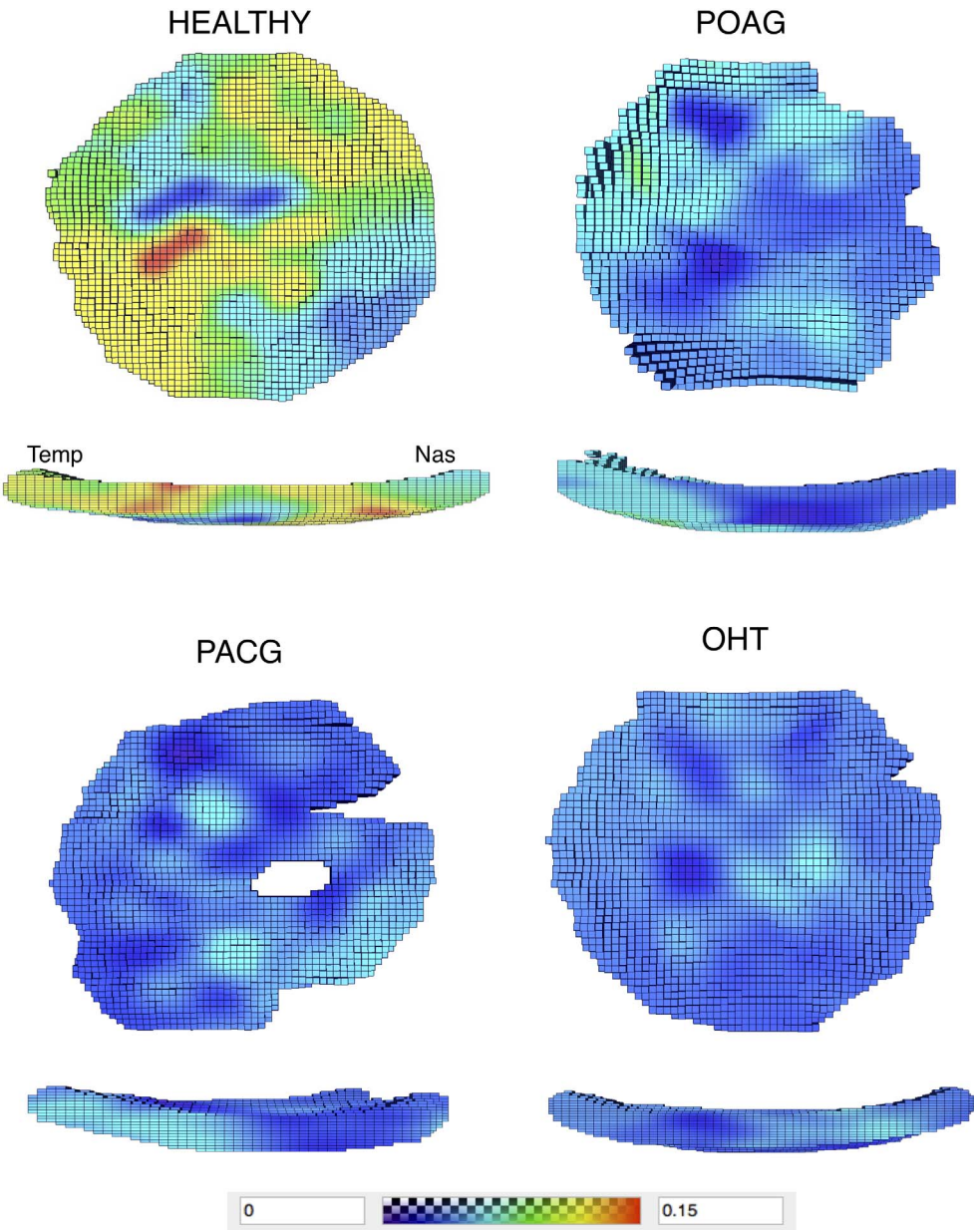

FIGURE 2. Representative color maps of acute IOP-induced effective strain superimposed on the LC geometry for healthy, POAG, PACG, and OHT subjects (first IOP elevation). Note that for each subject, one en face view and one midcoronal view (along nasal-temporal axis) of LC are shown. Note that the missing LC regions are due to poor LC visibility. Note that left eyes are flipped to right eye configuration. Nas, nasal; Temp, temporal.

to tease out these potential contributions and to confirm these initial results.

In this study, we found that some LCs displaced anteriorly or posteriorly, others displaced negligibly after IOP elevations. Such biomechanical variability has been demonstrated[20,27] in previous studies where IOP was lowered. Fazio et al.[28] have also demonstrated variability in axial LC displacement between African and European subjects. This suggests that multiple factors might play a complex role in governing the trends in axial displacements. We also found that axial LC displacements and strains in glaucoma subjects were similar to that in the healthy subjects. Low measures of lamina displacements in all subjects are in accordance with findings of previous studies.[16]

The strain levels exhibited by the POAG LCs and PACG LCs were found to be lower but not significantly different from those exhibited by the healthy LCs. It should be emphasized that most ONH biomechanics studies have reported significantly stiffer ONH connective tissues in glaucoma eyes,[29–31] and we might have expected to observe significantly smaller strains in glaucoma LCs using our strain mapping technique. However, our lack of significance could be due to several factors. First, we used a relatively small number of subjects in each group. Second, our recruited subjects were of Chinese ethnicity. It is currently unknown whether ONH biomechanics would be affected the same in Chinese subjects as in those from other ethnicities during the development and progression of glaucoma. For instance, strong differences have been observed between individuals of European and African descent.[28,32] Third, 67% of our POAG and PACG subjects had early glaucoma. Because ONH biomechanics is known to be affected differently during the different stages of glaucoma in

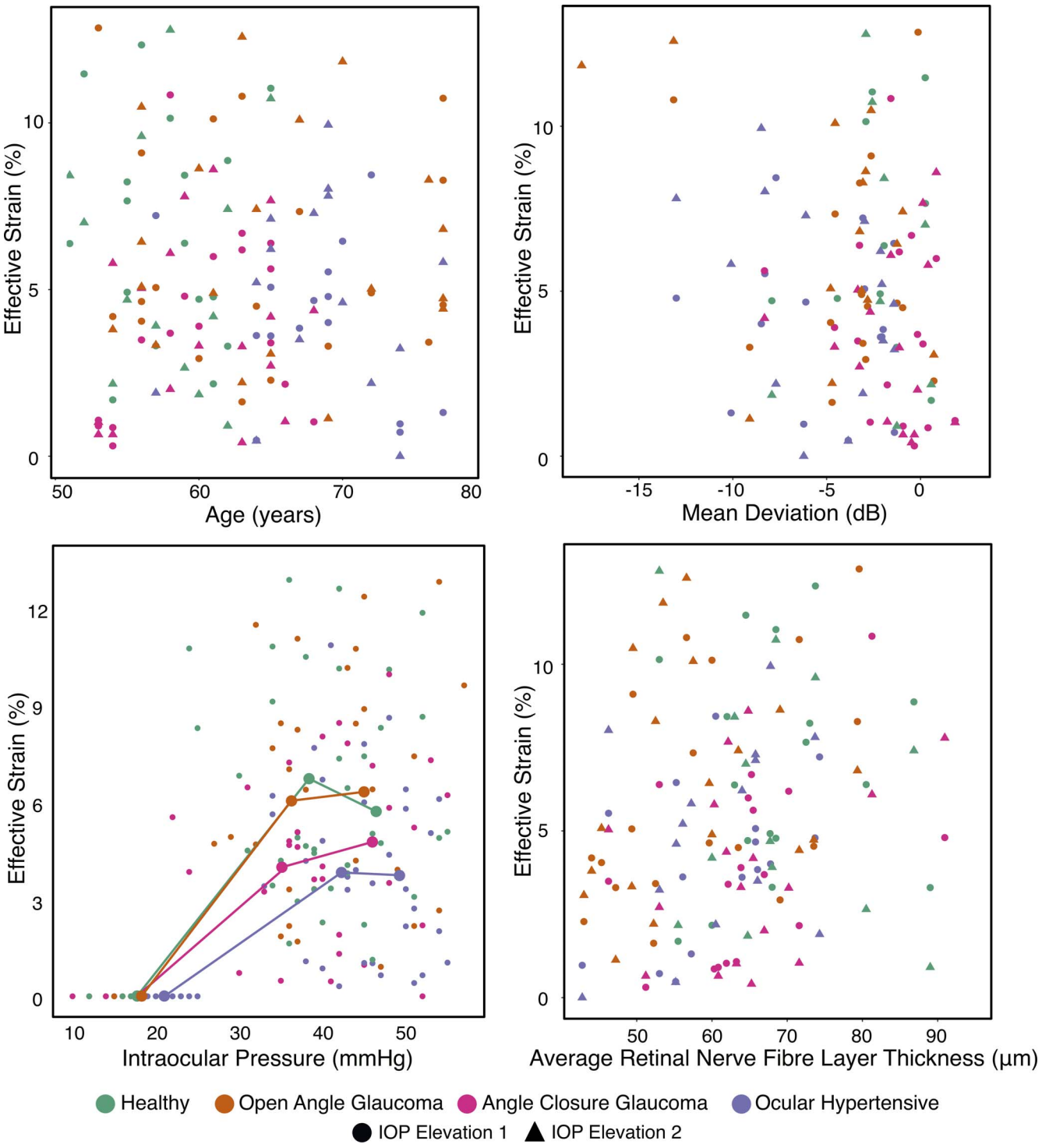

FIGURE 3. Scatterplots of acute IOP-induced LC effective strain (median) plotted against age, MD of visual field, IOP, and RNFL thickness, for IOP elevations to approximately 35 and approximately 45 mm Hg. The line plots (*bottom* graph) show the average values of effective strain (as shown in Table 1) for each IOP elevation for all subject groups.

monkeys,[33] the same could be true in humans. Fourth, PACG subjects were significantly older than healthy subjects (68 ± 5- vs. 58 ± 4-years old; $P < 0.05$). As age has a strong impact on ONH biomechanics,[34] this could also have been a limiting factor for our PACG group. It is also possible that the story is a lot more complex. For instance, there could be a scenario in glaucoma where changes in ONH tissue biomechanical properties would be accompanied with changes ONH morphology that would result in no LC strain changes with IOP. For instance, Roberts et al.[35] found that, in some cases, LC strains (estimated but not measured) in early glaucoma eyes were similar to those in healthy eyes.

In this population, we did not find an association between effective strain and visual field loss. The opposite was true in our previous study,[20] in which we measured LC strains induced by trabeculectomy. It is important to emphasize that

Table 2. Region-Wise Mean Effective Strain (%) for All Included Subjects

	Healthy		POAG		PACG		OHT	
Region Location	**IOP 1**	**IOP 2**	**IOP 1**	**IOP 2**	**IOP 1**	**IOP 2**	**IOP 1**	**IOP 2**
Temporal	6.17 ± 3.61	6.11 ± 3.09	5.29 ± 2.48*	6.26 ± 3.18	3.70 ± 2.38†	4.67 ± 2.57	3.90 ± 2.66	3.16 ± 2.25
Supero-temporal	6.25 ± 3.36	5.59 ± 3.40	5.65 ± 2.66	6.39 ± 3.47	4.29 ± 3.21	4.52 ± 2.62	3.48 ± 2.46‡	3.38 ± 2.95
Superior	6.96 ± 3.31	5.10 ± 2.60	6.20 ± 3.69	6.24 ± 3.74	4.20 ± 2.86	4.52 ± 2.63	4.19 ± 2.62	4.21 ± 3.28
Supero-nasal	6.99 ± 2.61	4.92 ± 2.68	6.80 ± 3.82	6.32 ± 3.64	3.70 ± 2.26	5.22 ± 3.09	4.72 ± 3.02	4.63 ± 3.49
Nasal	5.96 ± 2.52	5.84 ± 2.91	6.67 ± 4.42	6.45 ± 4.17	4.10 ± 2.70	4.83 ± 3.15	5.70 ± 3.74§	4.38 ± 3.98
Infero-nasal	5.96 ± 3.00	5.07 ± 2.33	6.10 ± 3.94	6.41 ± 3.68	3.43 ± 2.31	5.77 ± 4.79	4.83 ± 4.64	3.09 ± 2.75
Inferior	6.80 ± 3.43	6.87 ± 3.64	5.14 ± 3.00*	5.99 ± 3.03	3.07 ± 1.69||	4.24 ± 3.16	5.63 ± 3.37	3.36 ± 2.37
Infero-temporal	7.11 ± 3.84	6.86 ± 3.27	4.97 ± 2.58*	5.88 ± 3.12	3.52 ± 1.83||	4.82 ± 2.56	4.57 ± 3.09	3.14 ± 2.13

* *P* value is significant between supero-nasal and temporal, infero-temporal, and inferior regions.
† *P* value is significant between temporal and supero-temporal and superior regions.
‡ *P* value is significant between supero-temporal and superior, inferior, nasal, supero-nasal, and infero-nasal regions.
§ *P* value is significant between nasal, infero-nasal and superior, inferior, temporal, supero-temporal, and infero-temporal regions.
|| *P* value is significant between infero-temporal, inferior, and superior.

both studies had a different experimental design and they did not measure the same 'kind' of strain. In this study, we measured effective strains following an acute elevation in IOP. In our previous study, we measured effective strain relief following a decrease in IOP (as a result of trabeculectomy). Because we are dealing with soft tissues that are viscoelastic, there may not be any equivalence between the strains due an IOP decrease and those due to an IOP increase. A larger population and a longitudinal study may be required to tease out any relationships between strain and functional loss, if those were to exist. For any given group, we also found no associations between effective strain and the magnitude of IOP increase (first or second increment) suggesting variability in ONH biomechanics across subjects as previously reported.[20] Interestingly, we found that effective strain was positively associated with RNFL thickness for the first IOP elevation. However, this result may not be too surprising because our glaucoma subjects exhibited smaller RNFL thickness (Table 1) and on average, the glaucoma LCs deformed less than those of healthy subjects.

In POAG subjects, infero-temporal and temporal regions of the LCs were found to exhibit low strain. This finding could plausibly be explained by high collagen fiber alignment that has been reported in the infero-temporal (IT) ex vivo glaucoma LCs.[36] This high degree of fiber alignment in the IT region could possibly resist pressure-induced deformation better than other parts of the LC and thereby make the LC exhibit the lowest strain in events of acute IOP increase. However, it is not clear if this pattern of strain is an indicator of region specific disease susceptibility or marker of glaucoma progression or a compensation mechanism due to certain changes in the surrounding tissues. Our finding of low LC deformation in the IT regions contradicts the studies that have documented that the IT region is the most common site of clinical ONH damage in glaucoma.[37,38] This could be attributed to the progression of the disease and associated remodeling of the extracellular matrix, leading to a rapid change in tissue stiffness, and hence deformation pattern. It is possible that at high severity levels of the disease, the regional variation reverses itself with IT region exhibiting the highest deformation. Therefore, in-depth understanding of the regional biomechanical strain pattern in the LC accompanied by measure of glaucoma progression requires longitudinal data from subjects.

In OHT subjects, we found significantly lower LC deformation in the superior, supero-temporal, temporal than in the infero-temporal, inferior regions, and infero-nasal region. This suggests that low levels of strain are diffused over large areas of the LC. This diffuse strain pattern resembles the diffuse structural changes reported in the ocular hypertensive ONHs.[7,39,40]

We believe that it is important for us to put our work in perspective with other ex vivo studies that mapped peripapillary scleral and LC strains. Peripapillary scleral strains have been measured with electronic speckle pattern interferometry,[41–46] digital image correlation,[47–49] or optical flow.[50] LC strains have been mapped with phase-contrast micro-computed tomography imaging,[29,49,51] second harmonic generation imaging,[52,53] or laser scanning confocal microscopy.[54] Out of those studies, Fazio et al.[45] reported that the infero-temporal scleral sector exhibited the highest IOP-induced tensile strain in human donor eyes. This trend was also observed in human donor LCs by Midgett et al.,[52] but not in our study. We believe this is because ex vivo and in vivo biomechanical tests present inherent differences. First, ex vivo experiments on the LC have been carried out at a much higher resolution than OCT. This means that ex vivo LC strains may be more representative of the LC microstructure than in vivo strains. Second, ex vivo experiments come with a much better control of loads (e.g., IOP) and thus viscoelastic effects and their influence can also be assessed. This is not the case in vivo. Third, a majority of ex vivo studies have only considered IOP as the ONH load (except for a study by Feola et al.[55] that also considered the CSFP), while in vivo, the ONH is exposed to several loads, including IOP, CSFP, and the optic nerve traction.[10,11] It would therefore be plausible to expect considerable differences between ex vivo and in vivo strains. In fact, during in vivo OCT imaging, the ONH is likely to be prestretched due to an approximately 10° adduction angle causing optic nerve tension as discussed in Wang et al.[10] In live monkeys, the LC can also exhibit considerable CSFP-induced strains.[56] Such loads are rarely considered in ex vivo settings. In all, we believe it should not be surprising to find significant differences between ex vivo and in vivo strains. We also believe that both approaches are needed to fully understand the role of ONH biomechanics in glaucoma.

Several limitations warrant further discussion. First, it is important to mention that, based on this study alone, we cannot claim that OHT eyes are stiffer than healthy eyes. As previously mentioned, low IOP-induced LC strains could be explained by phenomena other than stiff connective tissues, such as high CSFP,[26] or a nontortuous optic nerve (that could make the ONH stiff due to optic nerve traction during OCT imaging).[10] Furthermore, our study was cross-sectional and our study population was small, which is a strong limitation. We may have studied OHT eyes that were stiff to start with, and

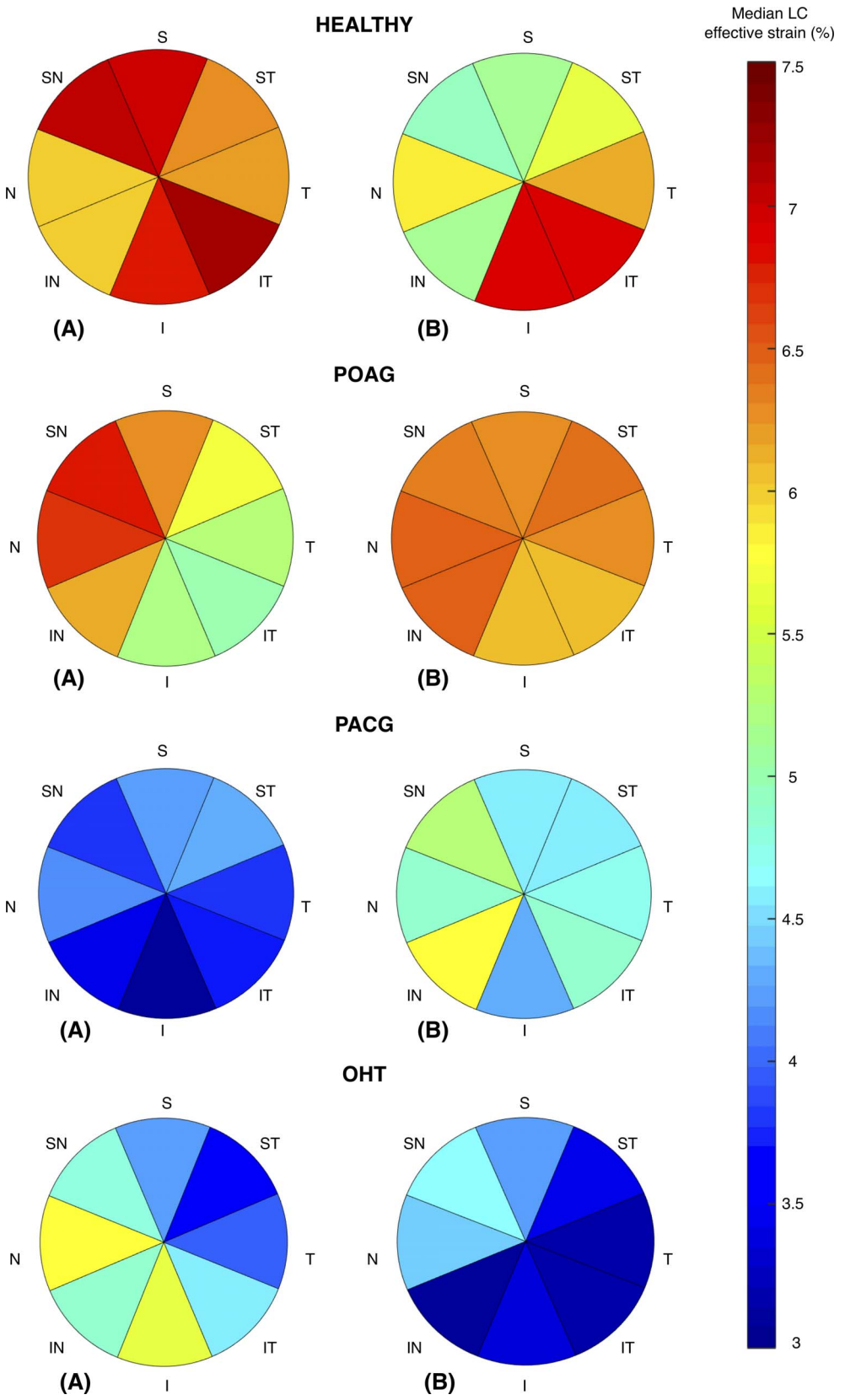

FIGURE 4. Mean octant-wise lamina cribrosa effective strain in Healthy, POAG, PACG, and OHT eyes at (**A**) IOP elevation to 35 mm Hg and (**B**) IOP elevation to 45 mm Hg. Healthy subjects show larger strain all over the LC than POAG, PACG, and OHT subjects. POAG subjects show significant ($P < 0.05$) regional variation, with infero-temporal sector showing lowest deformation. PACG subjects also show low strain in the inferior, temporal, and infero-temporal sectors. On the contrary, LCs of the OHT subjects show a diffuse pattern of low strain as compared with other subject groups, with lowest deformation ($P < 0.05$) in the supero-temporal, temporal, superior, and infero-temporal octants.

Investigative Ophthalmology & Visual Science

OHT eyes that were at different stages of their extracellular matrix remodeling process. In other words, we may not have captured the full biomechanical spectrum of ocular hypertension. When monkeys were exposed to chronic IOP elevations, it was consistently demonstrated that their eyes went through a phase of connective tissue hypercompliance before becoming stiff.[33] It is highly plausible that this same phenomenon would occur in humans but this has yet to be proven, and our study was not designed to capture such a phenomenon as we merely reported cross-sectional strains. Proving hypercompliance in humans would require a much larger population of OHT subjects that would be followed longitudinally for many years until some of them progress into glaucoma. In practice, any longitudinal glaucoma study is difficult to achieve, and this may need a strong collaborative effort from the entire glaucoma community. Nevertheless, we strongly believe that our work is still an important and necessary first step to potentially understand the role of connective tissues in glaucoma in humans. We are hoping our work will motivate larger cross-sectional and new longitudinal studies about ONH biomechanics in humans.

Second, it should be emphasized that in vivo biomechanical tests in patients, as performed herein, represent certain clinical challenges. As opposed to ex vivo biomechanical testing, it is very difficult to exactly control the 'starting' IOP and the exact amount of IOP increase. Because ocular collagenous tissues are known to exhibit nonlinear strains with IOP,[50,57] it then becomes difficult to compare strains across groups that have differing baseline IOPs. This problem is also intrinsic to in vivo biomechanical testing of the cornea but has often been ignored. To overcome this issue during the implementation of our experimental design, we have tried to: (1) recruit subjects with similar baseline IOPs, and (2) apply relatively high IOP elevations of 20 and 30 mm Hg with ophthalmodynamometry. However, we were not able to recruit OHT and healthy subjects with similar baseline IOPs; on average, baseline IOP was 17 mm Hg in healthy subjects, and 21 mm Hg in OHT subjects. To overcome this effect, we treated baseline IOP as a confounding variable in the statistical analysis, and found that LC strains in OHT subjects were significantly smaller than those in healthy subjects for the first IOP elevation. Finally, it is worth mentioning that if one were to vertically translate the strain-IOP curve of healthy subjects (from Fig. 3) to start at IOP = 21 mm Hg for 0% strain (i.e., same starting point as for OHT subjects), one would still observe a stiffer strain-IOP response in OHT subjects. In all, we believe our data support the fact that OHT subjects exhibit low strains but validations in larger populations should be carried out.

Third, OCT scans were typically acquired 2 to 3 minutes post-IOP elevation, thus providing a relatively short time duration for the ONH to deform. For some eyes, this short duration might not be enough for the IOP to set off all the mechanical changes that deforms the ONH to the maximum (at the applied IOP). Therefore, it is possible that in some patients, the OCT scan was acquired before the tissues reached their maximum deformation. However, our IOP elevation protocol was kept consistent for all patients.

Fourth, because LC visibility varies between eyes and potentially between groups, it is possible that we compared different regions of the LC across groups. To limit this effect, we first reconstructed all LCs with a constant depth of 135 μm. For our sectorial analyses, we excluded LC sectors with <50% visibility. In order to remove bias caused by LC transverse visibility in our "full-LC" strain comparisons, we investigated a separate approach. Because peripheral LC visibility is typically poor in a majority of LCs, we decided to focus on the central region with a stricter criterion for LC visibility. The central LC region was defined as a circular region (covering an area that represented ~50% of the LC). The center of the region was that of BMO projected onto the anterior LC surface. The radius of the region was equal to half the mean of the semiminor and semimajor axes of the best ellipse fit to the outer edge of the LC. When we included LCs with >70% visibility in the central region (as opposed to >60% for full LCs in our previous analyses), our conclusions remained the same. The median effective strains for each group were similar (healthy: 7.4%, POAG: 5.73%, PACG: 3.89%, OHT: 3.79%), and effective strains in OHT subjects were also found to be significantly lower than those in healthy subjects ($P = 0.034$). Unfortunately, any stricter criteria (>80% or >90% visibility in the central LC) required us to exclude more than half of the subjects (with a very high number of healthy subjects), which was deemed inappropriate.

Fifth, our study was limited to a small group of subjects in each diagnostic group. Although, we could report intergroup and regional difference in strain, studying a larger number of subjects would be of interest.

Sixth, the glaucoma subjects in this study were administered with subject-specific pharmacologic treatment for IOP reduction before recruitment. Such a treatment may have altered the biomechanical properties of the ONH, and further studies about these effects are warranted.

Seventh, the LC strains we reported correspond to IOPs of approximately 35 and 45 mm Hg. It is plausible that a certain group of glaucoma subjects would never reach those IOPs for long periods of time. In other words, the strains we measured may not be the same strains that could trigger glaucoma damage. Future work should be warranted to measure LC strains for smaller IOP elevations.

Eighth, in this work we chose to report effective strain in the LC (rather than all other strain components) because (1) in our previous strain mapping study,[20] we found that effective strain (but not the first and third principal components) was associated with visual field loss; and because (2) it is a single number that provides a summary of all other six strains components. However, further studies should be carried out to understand the implication of each strain component in the development and progression of glaucoma.

Ninth, we cannot exclude that compression of blood vessels in the lamina cribrosa (mostly microcapillaries) following acute IOP elevations contributed to the observed LC strains. We believe this contribution is likely to be small as collagen and axons, but not blood, constitute the vast majority of the LC. However, further studies will be required to better understand this contribution.

Tenth, it is possible that a change in ocular perfusion (as could occur with a change of IOP) may affect OCT image quality and attenuation, and may thus impact the performance of our 3D tracking algorithm. To limit these effects we have postprocessed all OCT volumes using adaptive-compensation to 'harmonize' image quality in undeformed and deformed OCT volumes. This approach worked successfully in our previous in vivo strain mapping studies.[10,20] However, more work may be required to fully understand the effects of a change in ocular perfusion on OCT image quality.

Eleventh, it has been shown that the LC exhibits significant remodeling during the development and progression of glaucoma, which can lead to outward migration of the anterior and posterior LC insertion points.[58–61] This may result in a change of biomechanical environment for the LC. It is therefore plausible that IOP-induced LC strains would be highly dependent on the insertion position of the LC into the sclera (or the pia). We have not yet looked for such associations.

Investigative Ophthalmology & Visual Science

Twelfth, we found that LC strains for the second IOP elevation were lower than those for the first IOP elevation. On average this was true for the healthy and OHT groups. This may appear counterintuitive as for most ex vivo experiments with ocular tissues, strains should increase with IOP. We believe, it could be that: (1) each eye may not have followed the same elastic path during consecutive IOP loadings with the ophthalmodynamometer. This is because after the first indentation, the ophthalmodynamometer was removed from the eye and reapplied to generate a higher force for the second indentation. (2) Viscoelastic effects may have played a role during the entire biomechanical testing. Unfortunately, it is currently not possible to measure such effects in vivo with OCT. (3) Other in-vivo loads acting on the ONH (such as the CSFP or the optic nerve traction) may have changed in between the two IOP loading sessions. Because of the in vivo nature of the tests we performed, it is currently extremely hard to tease out such contributions. In the future, it may be worth to compare our strain results with those obtained with different means of changing IOP (e.g., water test, pharmacologic treatment).

Thirteenth, we were not able to recruit normal tension glaucoma subjects for this study. Such subjects should be considered for future studies as the biomechanics of their ONH might potentially explain why they develop glaucoma at normal levels of IOP.

In conclusion, we present a novel study that can map 3D local deformations of the human LC as a response to acute IOP elevation in vivo. We demonstrate that such LC deformations can be differentiated between healthy and ocular hypertensive subjects. We further demonstrate regional variations in local LC deformations, which may have implications for the development of the pattern of visual field loss in glaucoma.

Acknowledgments

The authors thank Thierry Chabin, ophthalmologist, MD, Sainte-Foy-Lès-Lyon, France, for providing the ophthalmodynamometer used in this study.

Supported by grants from the National University of Singapore (NUS) Young Investigator Award Grant NUSYIA_FY13_P03; R-397-000-174-133 (MJAG; Singapore); Ministry of Education, Academic Research Funds Tier 1 Grant R-397-000-181-112 (MJAG; Singapore); National Medical Research Council Grant NMRC/STAR/0023/2014 (TA; Singapore); and the National Institute for Health Research Biomedical Research Centre, Moor- fields Eye Hospital National Health Service Foundation Trust and University College London (UCL) Institute of Ophthalmology (NGS; London, UK).

Disclosure: **M.R. Beotra**, None; **X. Wang**, None; **T.A. Tun**, None; **L. Zhang**, None; **M. Baskaran**, None; **T. Aung**, None; **N.G. Strouthidis**, None; **M.J.A. Girard**, None

References

1. Quigley HA, Dunkelberger GR, Green WR. Retinal ganglion cell atrophy correlated with automated perimetry in human eyes with glaucoma. *Am J Ophthalmol*. 1989;107:453–464.
2. Foster PJ, Buhmann R, Quigley HA, Johnson GJ. The definition and classification of glaucoma in prevalence surveys. *Br J Ophthalmol*. 2002;86:238–242.
3. Morgan WH, Yu DY, Balaratnasingam C. The role of cerebrospinal fluid pressure in glaucoma pathophysiology: the dark side of the optic disc. *J Glaucoma*. 2008;17:408–413.
4. Leibowitz HM, Krueger DE, Maunder LR, et al. The Framingham Eye Study monograph: an ophthalmological and epidemiological study of cataract, glaucoma, diabetic retinopathy, macular degeneration, and visual acuity in a general population of 2631 adults, 1973-1975. *Surv Ophthalmol*. 1980;24(suppl):335–610.
5. Quigley HA, Enger C, Katz J, et al. Risk factors for the development of glaucomatous visual field loss in ocular hypertension. *Arch Ophthalmol*. 1994;112:644–69.
6. Burgoyne CF, Downs JC, Bellezza AJ, et al. The optic nerve head as a biomechanical structure: a new paradigm for understanding the role of IOP-related stress and strain in the pathophysiology of glaucomatous optic nerve head damage. *Prog Retin Eye Res*. 2005;24:39–73.
7. Sullivan-Mee M. The role of ocular biomechanics in glaucoma management: understanding the role of ocular biomechanical properties may be key in the future of glaucoma management. Here's why. *Review of Optometry*. 2008;145.
8. Sigal IA, Ethier CR. Biomechanics of the optic nerve head. *Exp Eye Res*. 2009;88:799–807.
9. Wang N, Xie X, Yang D, et al. Orbital cerebrospinal fluid space in glaucoma: the Beijing Intracranial and Intraocular Pressure (iCOP) study. *Ophthalmology*. 2012;119:2065–2073.e1.
10. Wang X, Beotra MR, Tun TA, et al. In vivo 3-dimensional strain mapping confirms large optic nerve head deformations following horizontal eye movements. *Invest Ophthalmol Vis Sci*. 2016;57:5825–5833.
11. Wang X, Rumpel H, Lim WEH, et al. Finite element analysis predicts large optic nerve head strains during horizontal eye movementseye movements induce optic nerve head strains. *Invest Ophthalmol Vis Sci*. 2016;57:2452–2462.
12. Demer JL. Optic nerve sheath as a novel mechanical load on the globe in ocular ductionoptic nerve sheath constrains duction. *Invest Ophthalmol Vis Sci*. 2016;57:1826–1838.
13. Strouthidis NG, Girard MJ. Altering the way the optic nerve head responds to intraocular pressure-a potential approach to glaucoma therapy. *Curr Opin Pharmacol*. 2013;13:83–89.
14. Strouthidis NG, Fortune B, Yang H, et al. Effect of acute intraocular pressure elevation on the monkey optic nerve head as detected by spectral domain optical coherence tomography. *Invest Ophthalmol Vis Sci*. 2011;52:9431–9437.
15. Lee EJ, Kim TW, Weinreb RN. Reversal of lamina cribrosa displacement and thickness after trabeculectomy in glaucoma. *Ophthalmology*. 2012;119:1359–1366.
16. Agoumi Y, Sharpe GP, Hutchison DM, et al. Laminar and prelaminar tissue displacement during intraocular pressure elevation in glaucoma patients and healthy controls. *Ophthalmology*. 2011;118:52–59.
17. Tun TA, Thakku SG, Png O, et al. Shape changes of the anterior lamina cribrosa in normal, ocular hypertensive, and glaucomatous eyes following acute intraocular pressure elevation acute IOP-induced lamina cribrosa shape changes. *Invest Ophthalmol Vis Sci*. 2016;57:4869–4877.
18. Thakku SG, Tham Y-C, Baskaran M, et al. A global shape index to characterize anterior lamina cribrosa morphology and its determinants in healthy indian eyes LC-GSI to characterize LC morphology. *Invest Ophthalmol Vis Sci*. 2015;56:3604–3614.
19. Girard MJ, Strouthidis NG, Desjardins A, et al. In vivo optic nerve head biomechanics: performance testing of a three-dimensional tracking algorithm. *J R Soc Interface*. 2013;10:20130459.
20. Girard MJ, Beotra MR, Chin KS, et al. In vivo 3-dimensional strain mapping of the optic nerve head following intraocular pressure lowering by trabeculectomy. *Ophthalmology*. 2016;123:1190–1200.
21. Girard MJ, Tun TA, Husain R, et al. Lamina cribrosa visibility using optical coherence tomography: comparison of devic-

es and effects of image enhancement techniques. *Invest Ophthalmol Vis Sci*. 2015;56:865–874.

22. Girard MJ, Strouthidis NG, Ethier CR, Mari JM. Shadow removal and contrast enhancement in optical coherence tomography images of the human optic nerve head. *Invest Ophthalmol Vis Sci*. 2011;52:7738–7748.
23. Girard MJA, Downs JC, Bottlang M, et al. Peripapillary and posterior scleral mechanics—part ii: experimental and inverse finite element characterization. *J Biomech Eng*. 2009;131:051012.
24. Eilaghi A, Flanagan JG, Simmons CA, Ethier CR. Effects of scleral stiffness properties on optic nerve head biomechanics. *Ann Biomed Eng*. 2010;38:1586–1592.
25. Grytz R, Meschke G, Jonas JB. The collagen fibril architecture in the lamina cribrosa and peripapillary sclera predicted by a computational remodeling approach. *Biomech Model Mechanobiol*. 2011;10:371–382.
26. Jonas JB, Wang N, Wang YX, et al. Ocular hypertension: general characteristics and estimated cerebrospinal fluid pressure. The Beijing Eye Study 2011. *PLoS One*. 2014;9: e100533.
27. Quigley H, Arora K, Idrees S, et al. Biomechanical responses of lamina cribrosa to intraocular pressure change assessed by optical coherence tomography in glaucoma eyes. *Invest Ophthalmol Vis Sci*. 2017;58:2566–2577.
28. Fazio MA, Johnstone JK, Smith B, et al. Displacement of the lamina cribrosa in response to acute intraocular pressure elevation in normal individuals of african and european descent. *Invest Ophthalmol Vis Sci*. 2016;57:3331–3339.
29. Hommer A, Fuchsjäger-Mayrl G, Resch H, et al. Estimation of ocular rigidity based on measurement of pulse amplitude using pneumotonometry and fundus pulse using laser interferometry in glaucoma. *Invest Ophthalmol Vis Sci*. 2008;49:4046–4050.
30. Roberts MD, Sigal IA, Liang Y, et al. Changes in the biomechanical response of the optic nerve head in early experimental glaucoma. *Invest Ophthalmol Vis Sci*. 2010; 51:5675–5684.
31. Downs JC, Roberts MD, Burgoyne CF. The mechanical environment of the optic nerve head in glaucoma. *Optom Vis Sci*. 2008;85:425–435.
32. Girkin CA, Fazio MA, Yang H, et al. Variation in the three-dimensional histomorphometry of the normal human optic nerve head with age and race: lamina cribrosa and peripapillary scleral thickness and position. *Invest Ophthalmol Vis Sci*. 2017;58:3759–3769.
33. Yang H, Reynaud J, Lockwood H, et al. The connective tissue phenotype of glaucomatous cupping in the monkey eye - clinical and research implications. *Prog Retin Eye Res*. 2017;59(suppl c):1–52.
34. Burgoyne CF. A biomechanical paradigm for axonal insult within the optic nerve head in aging and glaucoma. *Exp Eye Res*. 2011;93:120–132.
35. Yang H, Thompson H, Roberts MD, et al. Deformation of the early glaucomatous monkey optic nerve head connective tissue after acute IOP elevation in 3-D histomorphometric reconstructions. *Invest Ophthalmol Vis Sci*. 2011;52:345–363.
36. Jones HJ, Girard MJ, White N, et al. Quantitative analysis of three-dimensional fibrillar collagen microstructure within the normal, aged and glaucomatous human optic nerve head. *J R Soc Interface*. 2015;12:20150066.
37. Kamal DS, Viswanathan AC, Garway-Heath DF, Hitchings RA, Poinoosawmy D, Bunce C. Detection of optic disc change with the Heidelberg retina tomograph before confirmed visual field change in ocular hypertensives converting to early glaucoma. *Br J Ophthalmol*. 1999;83: 290–294.
38. Strouthidis NG, Gardiner SK, Sinapis C, et al. The spatial pattern of neuroretinal rim loss in ocular hypertension. *Invest Ophthalmol Vis Sci*. 2009;50:3737–3742.
39. Pederson JE, Anderson DR. The mode of progressive disc cupping in ocular hypertension and glaucoma. *Arch Ophthalmol*. 1980;98:490–495.
40. Tuulonen A, Airaksinen PJ. Initial glaucomatous optic disk and retinal nerve fiber layer abnormalities and their progression. *Am J Ophthalmol*. 1991;111:485–490.
41. Girard MJA, Suh JKF, Bottlang M, et al. Scleral biomechanics in the aging monkey eye. *Invest Ophthalmol Vis Sci*. 2009; 50:5226–5237.
42. Girard MJA, Suh JKF, Bottlang M, et al. Biomechanical changes in the sclera of monkey eyes exposed to chronic IOP elevations. *Invest Ophthalmol Vis Sci*. 2011;52:5656–5669.
43. Fazio MA, Grytz R, Morris JS, et al. Human scleral structural stiffness increases more rapidly with age in donors of african descent compared to donors of European descent. *Invest Ophthalmol Vis Sci*. 2014;55:7189–7198.
44. Fazio MA, Bruno L, Reynaud JF, et al. Compensation method for obtaining accurate, sub-micrometer displacement measurements of immersed specimens using electronic speckle interferometry. *Biomed Optics Exp*. 2012;3:407–417.
45. Fazio MA, Grytz R, Bruno L, et al. Regional variations in mechanical strain in the posterior human sclera. *Invest Ophthalmol Vis Sci*. 2012;53:5326–5333.
46. Fazio MA, Grytz R, Morris JS, et al. Age-related changes in human peripapillary scleral strain. *Biomech Model Mechanobiol*. 2014;13:551–563.
47. Pyne JD, Genovese K, Casaletto L, Vande Geest JP. Sequential-digital image correlation for mapping human posterior sclera and optic nerve head deformation. *J Biomech Eng*. 2014;136:021002.
48. Coudrillier B, Tian J, Alexander S, et al. Biomechanics of the human posterior sclera: age- and glaucoma-related changes measured using inflation testing. *Invest Ophthalmol Vis Sci*. 2012;53:1714–1728.
49. Coudrillier B, Campbell IC, Read AT, et al. Effects of peripapillary scleral stiffening on the deformation of the lamina cribrosa. *Invest Ophthalmol Vis Sci*. 2016;57:2666–2677.
50. Girard MJ, Downs JC, Burgoyne CF, Suh JKF. Experimental surface strain mapping of porcine peripapillary sclera due to elevations of intraocular pressure. *J Biomech Eng*. 2008; 130:041017.
51. Coudrillier B, Geraldes DM, Vo NT, et al. Phase-contrast micro-computed tomography measurements of the intraocular pressure-induced deformation of the porcine lamina cribrosa. *IEEE Trans Med Imaging*. 2016;35:988–999.
52. Midgett DE, Pease ME, Jefferys JL, et al. The pressure-induced deformation response of the human lamina cribrosa: analysis of regional variations. *Acta Biomater*. 2017;53(suppl C):123–139.
53. Sigal IA, Grimm JL, Jan N-J, et al. Eye-specific IOP-induced displacements and deformations of human lamina cribrosa. *Invest Ophthalmol Vis Sci*. 2014;55:1–15.
54. Albon J, Purslow PP, Karwatowski WSS, Easty DL. Age related compliance of the lamina cribrosa in human eyes. *Br J Ophthalmol*. 2000;84:318.
55. Feola AJ, Coudrillier B, Mulvihill J, et al. Deformation of the lamina cribrosa and optic nerve due to changes in cerebrospinal fluid pressure CSFp effects on lamina cribrosa and optic nerve. *Invest Ophthalmol Vis Sci*. 2017;58:2070–2078.
56. Sigal IA, Ethier CR. Biomechanics of the optic nerve head. *Exp Eye Res*. 2009;88:799–807.

Investigative Ophthalmology & Visual Science

57. Grytz R, Fazio MA, Girard MJA, et al. Material properties of the posterior human sclera. *J Mech Behav Biomed Mater*. 2014;29(suppl C):602–617.
58. Grytz R, Sigal IA, Ruberti JW, et al. Lamina cribrosa thickening in early glaucoma predicted by a microstructure motivated growth and remodeling approach. *Mech Mater*. 2012;44:99–109.
59. Yang H, Williams G, Downs JC, et al. Posterior (outward) migration of the lamina cribrosa and early cupping in monkey experimental glaucoma. *Invest Ophthalmol Vis Sci*. 2011;52:7109–7121.
60. Lee KM, Kim T-W, Weinreb RN, et al. Anterior lamina cribrosa insertion in primary open-angle glaucoma patients and healthy subjects. *PLoS One*. 2014;9:e114935.
61. Grytz R, Girkin CA, Libertiaux V, Downs JC. Perspectives on biomechanical growth and remodeling mechanisms in glaucoma. *Mech Res Commun*. 2012;42(suppl C):92–106.

Investigative Ophthalmology & Visual Science